Magnetic order in FeGaGe with interlaced quasi-one-dimensional Fe-Chains

Chenglin Shang(商成林),[1,*] Bingxian Shi(史秉贤),[1,*] Yangyang Fan(范洋洋),[1] Daye Xu(徐大业),[1] Juanjuan Liu(刘娟娟),[1] Jinchen Wang(汪晋辰),[1] Hongxia Zhang(张红霞),[1] Hongliang Wang(王洪亮),[2] Lijie Hao(郝丽杰),[2] and Peng Cheng(程鹏)[1,†]

[1] *Laboratory for Neutron Scattering and Key Laboratory of Quantum State Construction and Manipulation (Ministry of Education), School of Physics, Renmin University of China, Beijing 100872, China*

[2] *China Institute of Atomic Energy, PO Box-275-30, Beijing 102413, China*

We report the crystal growth, structural and physical properties of a rarely explored intermetallic compound FeGaGe. The main feature of its crystal structure is the formation of quasi-one-dimensional Fe chains in the *ab*-plane that are interlaced when viewed along the *c*-axis. Magnetization measurements reveal an antiferromagnetic transition at T_N=130 K. Upon further cooling, a susceptibility anomaly occurs at T^*=60 K which can be suppressed under high magnetic field indicating a possible crossover in spin order. Resistivity measurement shows metallic conductivity in FeGaGe with features at both T_N and T^*. Powder neutron diffraction experiment reveals a possible noncollinear spiral antiferromagnetic structure of FeGaGe with periodic spin modulation along the quasi-one-dimensional Fe-chains. Our results establish FeGaGe as a special magnetically ordered system that might host exotic quantum magnetic states.

PACS numbers: 75.50.Ee, 61.05.F-, 75.25.-j
Keywords: quasi-one-dimensional antiferromagnet, neutron scattering, magnetic structure

I. INTRODUCTION

When magnetic ions are aligned in some special lattice symmetry, the formation of exotic quantum phases of matter may be expected. For example, the ground state of geometrically frustrated spin systems with triangular or kagome lattices can host a quantum spin liquid[1–5] or a supersolid phase[6–9]. In honeycomb lattices such as α-$RuCl_3$, the Kitaev quantum spin liquid may be realized due to the bond-dependent anisotropic exchange interaction[10–12] as well as in recently discovered cobalt-based honeycomb magnets like $Na_2Co_2TeO_6$[13–15]. Materials with quasi-one-dimensional spin chains represent another important spin system, where exotic quantum states and magnetic excitations can emerge[16–22]. In the past few decades, much efforts have been devoted to exploring materials with the above lattice features aiming to discover or understand novel quantum magnetic states.

The research on quantum magnetism mainly focuses on insulators because the localized electrons would make the modeling of these spin systems much simpler. However in recent years, it has been shown that metallic magnets can also be a fertile playground for such research with important emergent quantum phenomena that cannot be realized in insulating systems. The main breakthrough is in kagome metals, besides geometric spin frustration, topological band structures accompanied by superconductivity, charge-density-waves and topological Hall effects have been discovered[23, 24]. Beyond kagome metals, recent studies of quasi-one-dimensional metallic magnets have revealed intriguing correlations between localized magnetic moments and itinerant electrons. For example, the quasi-one-dimensional Ce_3TiBi_5 exhibits antiferromagnetic order and anisotropic Kondo effect, highlighting the important role of electronic hybridiza-

* These authors contributed equally to this work
† Corresponding author: pcheng@ruc.edu.cn

tion [25]. More recently, an investigation of the metallic spin-chain material Ti_4MnBi_2 reveals that besides spinon excitations, three-dimensional conduction electrons become strongly correlated due to their coupling to one-dimensional (1D) magnetic moments[26, 27]. Therefore, it would be of great interest to seek new metallic 1D spin chain compounds that possibly favor a quantum critical point accompanied by emergent instabilities such as unconventional superconductivity.

Motivated by this, we have noticed an intermetallic compound FeGaGe. According to the record in the Inorganic Crystal Structure Database (ICSD), it has quasi-1D Fe-chains with a short intrachain Fe-Fe distance and a much larger interchain Fe-Fe distance. However its physical properties are nearly unknown, except that an early Mössbauer spectrum study showed it has an antiferromagnetic transition near 125 K[28]. Therefore, more structural and magnetic characterizations of FeGaGe are needed. It should also be mentioned that whether sizable single crystals of FeGaGe could be grown remains unknown.

In this study, the flux growth of millimeter-sized single crystals and preparation of polycrystalline samples of FeGaGe are reported. Through X-ray/neutron diffraction, magnetization, heat capacity and resistivity measurements on FeGaGe, its interlaced quasi-1D spin-chains, magnetic transition and possible non-collinear spiral antiferromagnetic structures are revealed. Our results have shown intriguing features of the magnetic order in FeGaGe that warrant further studies.

II. METHODS

Single crystals of FeGaGe were synthesized via a self-flux method. High-purity Fe powder, Ge powder, and bulk Ga in a molar ratio of 1:4:6 were mixed in an alumina crucible inside a quartz tube. All reagents were handled in an argon-filled glove box before the quartz tube was evacuated and sealed. The assembly was heated to 1050 °C and maintained at this temperature for 12 hours and then slowly cooled to 730 °C in a box furnace. The ampoule was subsequently removed from the furnace, inverted and centrifuged to remove the Ge-Ga flux from the crystals. Typical single-crystal dimensions were approximately 1 × 1 × 3 mm^3.

Polycrystalline samples of FeGaGe were fabricated using a solid-state reaction method with stoichiometric amounts Fe, Ga and Ge, similar to a previous report[28]. The reagents were mixed and placed in an alumina crucible and then sealed inside a quartz tube. The sealed assembly was heated to 650 °C and maintained at this temperature for 3 days. After cooling to room temperature, the product was thoroughly ground and pressed into a pellet, then resintered at the same temperature for an additional 4 days.

X-ray diffraction (XRD) data of FeGaGe powders were collected at room temperature using a Bruker D8 Advance X-ray diffractometer with Cu K_α radiation. The elemental composition of single crystals was examined with energy dispersive X-ray spectroscopy (EDX, Oxford X-Max 50). Magnetization data were collected on a Quantum Design Magnetic Property Measurement System (MPMS). The electrical transport measurements were carried out on a Quantum Design Physical Property Measurement System (PPMS-14T). The powder neutron diffraction experiments were carried out on the Xingzhi cold neutron triple-axis spectrometer at the China Advanced Research Reactor (CARR)[29]. About 2 grams of FeGaGe powder was used in the neutron experiments and the incident neutron energy was fixed at 16 meV.

The shape of FeGaGe single crystal is three-dimensional and irregular. In order to identify the crystal orientation, both X-ray Laue imaging and single-crystal XRD on some flat surface were performed. For different measurements/samples, it is hard to fix the magnetic field direction along a chosen crystallographic orientation (such as *c*-axis) due to the irregular crystal shape and the constraints of sample holder. However, we were able to determine/deduce

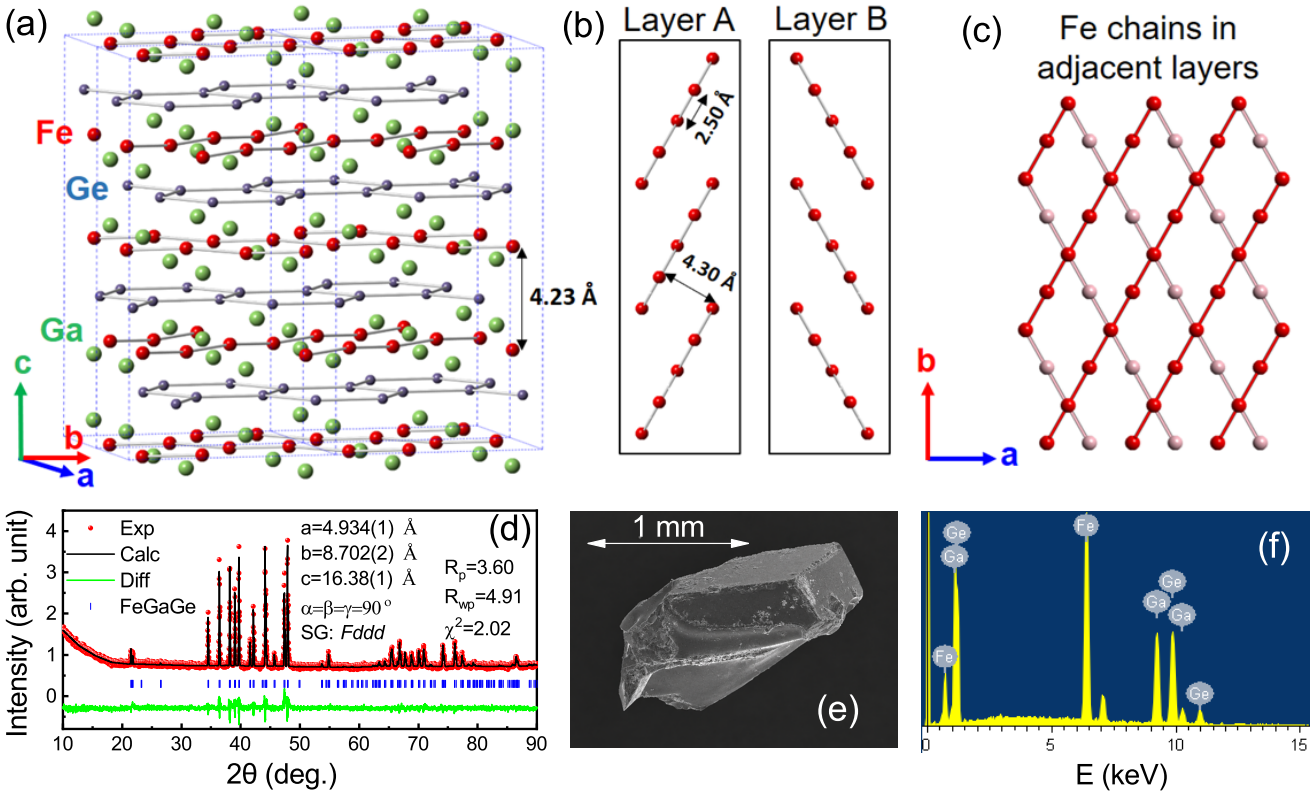


Fig. 1. Structural characterization of FeGaGe. (a) A sketch of the crystal structure of FeGaGe. Four unit cells illustrated by the blue dotted line are shown. The nearest Fe-Fe or Ga-Ga bonds are plotted, which show the quasi-1D or honeycomb lattice feature respectively. (b) The Fe chains in two adjacent layers along the *c*-axis are shown separately. (c) A view from *c*-axis on the Fe chains in two adjacent layers. Fe chains in different layers are shown in different colors (red and pink). (d) XRD patterns of FeGaGe powder and the Rietveld refinement result. (e) A SEM photo for a FeGaGe single crystal. (f) EDX spectroscopy of a FeGaGe single crystal.

Table I. Atomic coordinates of FeGaGe obtained from Rietveld refinement of the powder XRD data at room temperature. The values of occupancy were derived from refinement on the neutron diffraction data at 150 K.

atom	Wyckoff	occupancy	x	y	z
Ga	16g	0.676	0.1250	0.1250	0.0413(2)
Ge	16g	0.324	0.1250	0.1250	0.0413(2)
Fe	16g	1.000	0.1250	0.1250	0.4966(2)
Ga	16f	0.380	0.1250	0.4616(4)	0.1250
Ge	16f	0.620	0.1250	0.4616(4)	0.1250

all field directions for different measurement and specify them using [HKL] index. And the corresponding estimation error was given.

III. RESULTS AND DISCUSSIONS

A. Crystal structure and physical properties

According to an early report, FeGaGe adopts the orthorhombic $CuMg_2$-type structure with space group

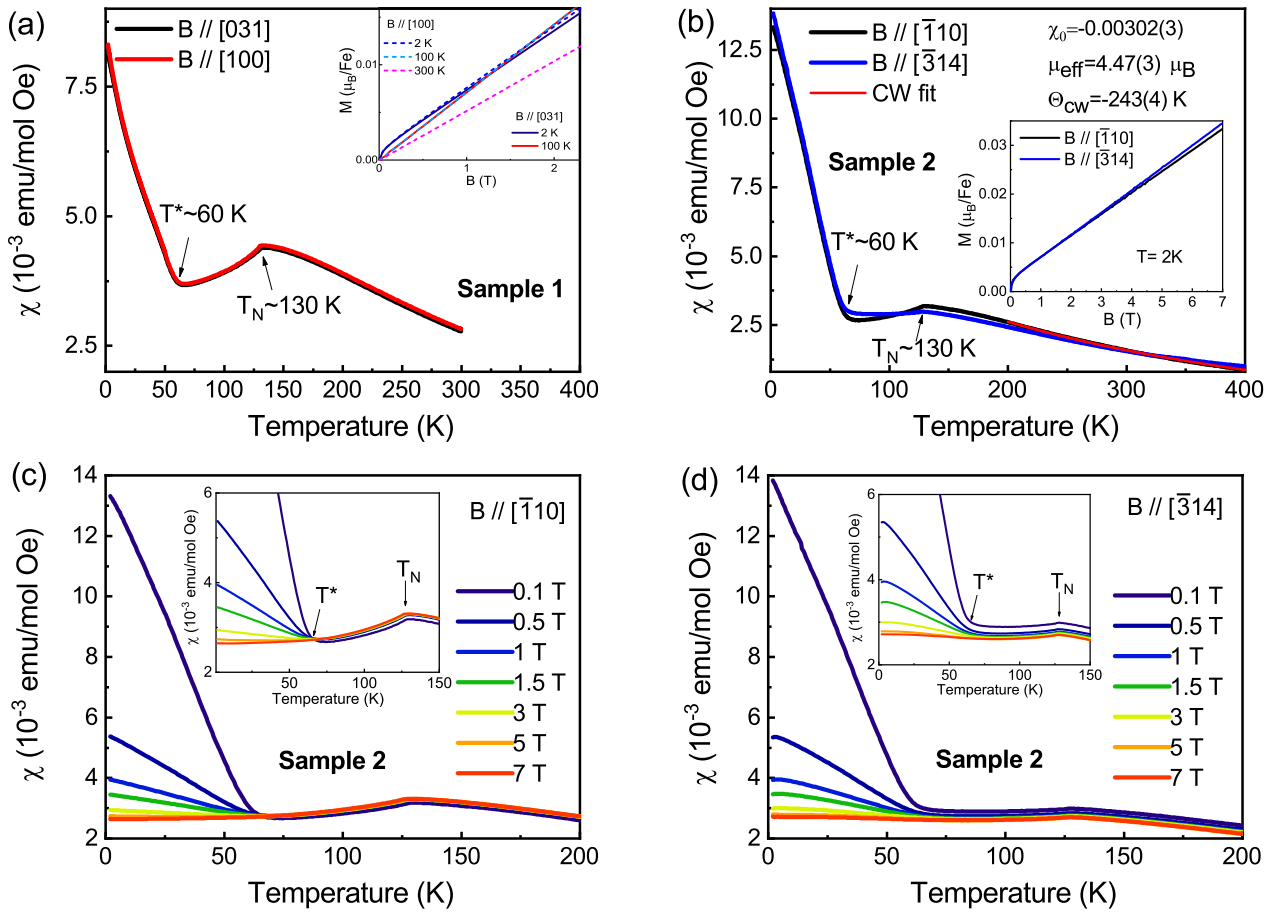


Fig. 2. Magnetization measurements of FeGaGe. Temperature-dependent magnetic susceptibility measured under a magnetic field of 0.1 T applied along different crystallographic orientation is shown in (a) and (b), the corresponding isothermal magnetization M(B) curves are shown in the insets. (c) and (d) show the temperature-dependent magnetic susceptibility measured under different field. The [$\bar{3}$14] orientation is 15 degrees away from *c*-axis. The insets shows enlarged views of the susceptibility data near T^*.

Fddd (No. 70). Fig. 1(d) presents the Rietveld refinement of the XRD pattern of FeGaGe powder, which confirms the same crystal structure determined previously[28]. The refined lattice parameters are shown in the inset of Fig. 1(d) and the atomic crystallographic data are shown in Table 1. It should be pointed out that since Ge and Ga have similar atomic numbers, it remains unclear whether site-mixing could occur between Ge and Ga from XRD refinement. For neutron scattering length, Ge and Ga have ∼12% difference. The refinement on neutron diffraction data of FeGaGe powders at 150 K gives an estimation of Ge/Ga site-mixing fraction, which is also shown in Table 1. However, the improvement of final agreement factors in this refinement is not appreciable, the values of occupancy in Table 1 can only be considered as a rough estimation. On the other hand, the EDX measurements on single crystals reveal consistent atomic ratio of Fe:Ge:Ga=1:1:1 [Fig. 1(f)], the relative errors are less than 3%. This result agrees with the Ge/Ga site-mixing fraction values refined by neutron data.

As illustrated in Fig. 1(a-c), the main feature in

the crystal structure of FeGaGe is the quasi-1D Fe chains. Within one layer in the *ab*-plane, quasi-1D Fe chains are parallel to each other with intrachain Fe-Fe distance of 2.50 Åand an interchain Fe-Fe distance of 4.30 Å[Fig. 1(b)]. In adjacent layers, the directions of Fe chains have an intersection angle of 60 degrees and the nearest interlayer Fe-Fe distance is 4.23 Å. Such short intrachain Fe-Fe distance indicates the formation of metal-metal bonding and makes FeGaGe a quasi-1D spin chain system[30, 31]. For the Fe-chains in adjacent layers viewed along the *c*-axis, they form a pseudo-kagome lattice as shown in Fig. 1(c). Therefore, the interlaced distribution of Fe chains makes FeGaGe quite unique in all quasi-1D spin chain system. On the other hand, the Ge atoms constitute honeycomb lattice as shown in Fig. 1(a).

The results of magnetization measurements on two FeGaGe single-crystal samples are shown in Fig. 2. From the temperature-dependent magnetic susceptibility χ(T) curve in Fig. 2(a,b), an antiferromagnetic transition is identified at T_N∼130 K, slightly higher than 125 K that determined by Mössbauer spectroscopy[28]. Using equation $\chi = \chi_0 + C/(T - \theta_{CW})$, the Curie-Weiss (CW) fit of the χ(T) data from 200 K to 400 K yields an effective moment μ_{eff} = 4.47 μ_B/Fe and CW temperature θ_{CW} = −243 K. Although the fitted values show certain differences for different temperature range and sample, all the obtained effective moments are close to the $S = 2$ spin state for Fe^{2+} and the negative CW temperature implies dominant antiferromagnetic interactions in this compound.

With further decreasing temperature, χ(T) curve at 0.1 T have another anomaly which exhibits an upturn feature below T^*∼60 K. The isothermal magnetization M(B) at different temperatures are shown in the insets of Fig. 2(a,b). M(B) curves follow linear field dependence at 100 K and 300 K. Below T^* and at 2 K, the M(B) curve shows nonlinear field dependence below 1 T. Fig. 2(c,d) displays $\chi(T)$ curves under different field and the upturn feature below T^* is gradually suppressed by higher magnetic field. Furthermore, for the specific heat data shown in Fig. 3(a), no discernible anomaly is observed near T^*=60 K under magnetic fields of either 0 or 7 T, which rules out the possibility of bulk magnetic phase transition at T^*. However, the susceptibility behavior indicates a crossover in spin order such as a gradual spin-reorientation or spin-canting may exist at T^*. For example, the kagome metal FeGe has a well-known crossover from collinear A-type AFM structure to double-cone canted AFM structure at 60 K[32]. But no anomaly is observed in C_p(T) data at around 60 K for FeGe[33]. Similar crossover in spin order without a specific heat anomaly is also observed in $Sr_4Ru_3O_{10}$[34] and $Fe_{32+\delta}Ge_{35-x}Si_x$[35]. Additionally, although XRD refinement does not identify any impurity phase, one cannot completely rule out the possibility that T^* may originate from some minor ferromagnetic impurity.

The single-crystal magnetization data in Fig. 2 also reveals crucial information about the magnetic anisotropy of FeGaGe. When the magnetic field is parallel to the ab-plane(B∥[100] and B∥[$\bar{1}$10]) or is tilted by approximately 30 degrees from the ab-plane(B∥[031]), the susceptibility χ(T) exhibits a steeper decrease below T_N than that of B∥[$\bar{3}$14] whose direction is only 15 degrees away from the *c*-axis. This suggests a weak easy *ab*-plane magnetic anisotropy which also agrees with the magnetic structure determined by neutron diffraction that the main components of the spins lie within the *ab*-plane.

Next, the specific heat and resistivity data of FeGaGe single crystal are presented in Fig. 3. A lamda-shape peak appears at T_N comfirming the bulk antiferromagnetic transition. In the inset of Fig. 3(a), a linear fit to the C_p/T versus T^2 plot is shown. Based on $C_p/T = \beta T^2 + \gamma$, the obtained coefficients are $\beta = 0.57$ mJ mol^{-1} K^{-4} and $\gamma = 12.2$ mJ mol^{-1} K^{-2}. The Debye temperature is estimated to be 104 K for FeGaGe, and the value of electronic specific-heat coefficient γ indicates a moderate electron correlation in

this compound. In Fig. 3(b), FeGaGe exhibits typical metallic transport behavior and a kink at T_N. This kink is attributed to the suppression of spin-disorder scattering as the system enters the magnetically ordered state, reflecting a strong coupling between the complex magnetic order and itinerant electrons, a feature similarly in other noncollinear metallic antiferromagnets such as CrRhAs[36]. Another kink feature appears at ∼4 K which might be due to the superconducting transition of residual Ga-flux. The resistivity data ρ(T) under magnetic field of 7 T is also measured. Interestingly, the magnetoresistance (MR) is negligible above T^*∼60 K but positive MR becomes notable below T^*. MR is close to 4% at 2 K and 7 T. This observation demonstrate the influence of possible crossover in spin order at T^* on the electronic transport behavior.

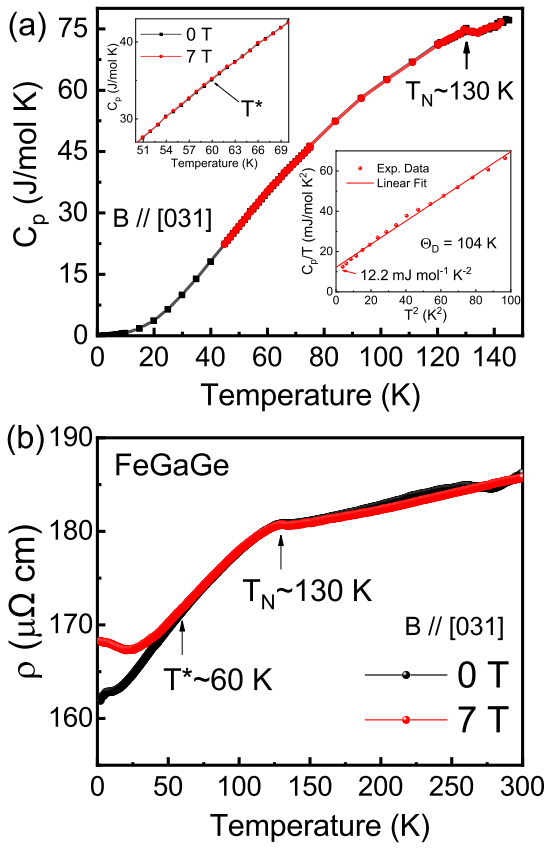


Fig. 3. (a) Temperature-dependent specific heat of FeGaGe measured under magnetic fields of 0 T and 7 T. The upper-left inset shows an enlarged view of the specific heat data near T^*, while the lower-right inset shows C_P/T as a function of T^2 in the low-temperature region together with a linear fit. (b) Temperature-depdendent resistivity of FeGaGe measured under magnetic fields of 0 T and 7 T.

B. Magnetic structure

To determine the ground-state magnetic structure of FeGaGe, powder neutron diffraction experiments were performed. Fig. 4(a) shows the raw data at 3.5 K and 150 K in the low-Q region. Two magnetic peaks can be identified and indexed as (1/3, 1/2, 0) and (1/3, 1/2, 2) respectively, which means that the magnetic structure should be best described by the propagation vector k=(1/3, 1/2, 0). Symmetry analysis was then performed using the $k-SUBGROUPSMAG$ tool from the Bilbao Crystallographic Server[37]. Based on the paramagnetic parent space group and the k vector, the group-subgroup hierarchy is obtained using ISODISTORT[38, 39]. It should be mentioned that for the parent $Fddd$ space group and k=(1/3, 1/2, 0), the star of k contains four arms: k_1=(1/3, 1/2, 0), $-k_1$=(-1/3, -1/2, 0), K_2=(1/3, -1/2, 0), $-k_2$=(-1/3, 1/2, 0). The two pairs (k_1, $-k_1$) and (k_2, $-k_2$) are inequivalent modulo reciprocal-lattice translations, while are related by a symmetry operation of the parent $Fddd$ space group. All the candidate magnetic models given by ISODISTORT simultaneously activate the two inequivalent k-pairs and therefore correspond to multi-k magnetic structures, rather than a single-k structure. Although a single-k state is not symmetry-forbidden, the multi-k spin configuration may host higher symmetry and is a more natural arrangement.

Subsequently, all six possible candidate magnetic space groups (MSGs) are $I_c222, I_c2_12_12_1, C_c2, C_a2, P_s\bar{1}$ and P_s1. The first two correspond to epikernels and possess more symmetry constraints than the other kernel MSGs. The MSG P_s1 represents the most complex combination of the irreducible representation (IR) basis modes

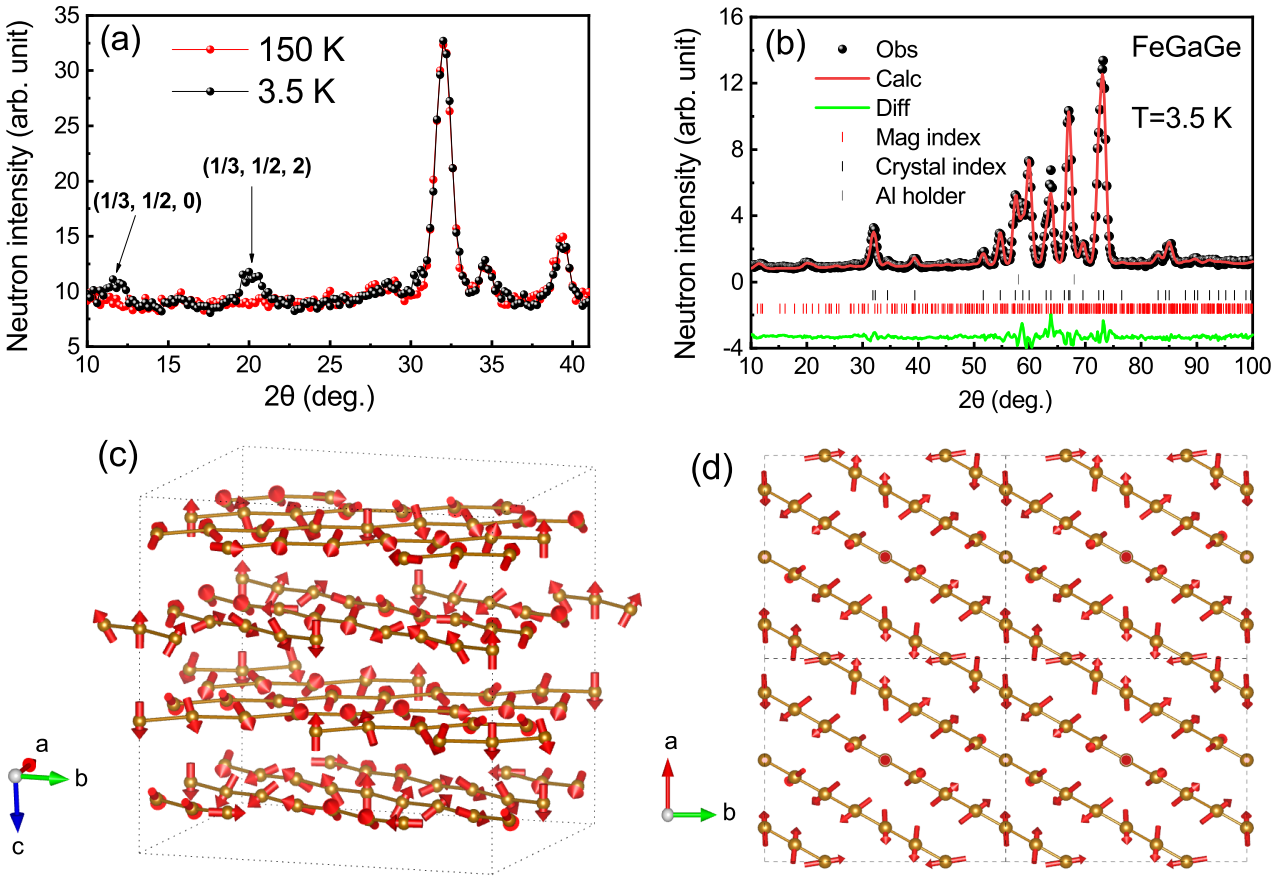


Fig. 4. Neutron diffraction and magnetic structure. (a) Powder neutron diffraction patterns of FeGaGe at 3.5 and 150 K in the low-angle range. The observed two magnetic Bragg peaks are indexed. (b) Rietveld refinement result for the neutron diffraction data at 3.5 K based on the magnetic structures plotted in (c) and (d). (c,d) Illustration of the low-temperature magnetic structure with only Fe atoms are visible. The black dashed lines indicate the magnetic unit cell and the nearest Fe-Fe bonds are plotted.

and thus exhibits the lowest symmetry among all MSGs. Both the refinements of nuclear and magnetic structure were performed using the JANA2020 package[40], our data show that the Rietveld refinements based on the IRs in the first two MSGs (I_c222 and $I_c2_12_12_1$) have much better final agreement R-factors than the others. This result aligns with the principle that usually magnetically ordered states tend to preserve higher symmetry as much as possible[41]. Table 2 shows the refinement result of three magnetic models with the best fit. Among them, the final agreement R-factors are similar.

Although Fe ions have only one Wyckhoff position in the paramagnetic crystal unit cell, they will occupy several different Wyckhoff positions for part of the above MSGs in the magnetic unit cell. This means that during the refinement, Fe ions in different Wyckhoff positions may have different magnitudes of the magnetic moment[42] due to the introduction of additional refinement parameters. For FeGaGe, since all the Fe ions have a similar ligand environment, it is physically reasonable to assume that they should have equal moment magnitudes. For each magnetic structural model, refinement results without any constraints (labeled as N/A) or constraining all Fe ions to have the same magnitude of the magnetic moment

Table II. Final agreement R-factors for the refinement of neutron data based on different MSG models.

Magnetic space group	Magnetic IR	Costraint	$R(All)$ (%)	$wR(All)$ (%)	R (nuc.) (%)	R (mag.) (%)	Minimum moment (μ_B/Fe)	Maximum Moment (μ_B/Fe)
I_c222	Γ_1	N/A	6.22	7.98	5.35	8.32	0.70 (18)	3.0 (3)
		M_{equal}	5.9	7.59	4.78	6.32	2.10 (13)	2.10 (13)
I_c222	Γ_2	N/A	6.09	7.87	5.17	7.58	2.0 (3)	4.0 (3)
		M_{equal}	5.84	7.53	4.84	6.20	2.10 (4)	2.10 (4)
$I_c2_12_12_1$	Γ_2	N/A	6.15	7.87	5.27	8.04	1.0 (3)	3.0 (2)
		M_{equal}	5.84	7.54	4.75	6.47	2.20 (19)	2.20 (19)

(labeled as M_{equal}) are both shown in Table 2. It can be seen that adding the equal moment constraint will improve the R-factors for all three models. Therefore we propose that the three magnetic models in Table 2 with M_{equal} constraint are plausible magnetic structures for FeGaGe.

Fig .4(c,d) display the magnetic structure of FeGaGe with the IR of Γ_1 and MSG I_c222 and the corresponding refined neutron data are presented in Fig. 4(b). The ordered magnetic moment of Fe ions is 2.10 ± 0.13 μ_B/Fe. This value is much smaller than the effective moment of Fe^{2+} in a theoretical localized model, but is quite close to those observed in many intermetallic antiferromagnets such as FeGe[32, 43]. This reduced moment value indicates the $3d$ electrons of Fe ions may not be fully localized and possibly exhibit itinerant magnetism[44–46]. It should be addressed that covalency or orbital hybridization between the $3d$ orbitals of Fe and the orbitals of neighboring Ga/Ge ions may result in reduced ordered moment as well. Quantum fluctuations and other many-body effects are also possible reasons. As illustrated in Fig. 4(c,d), the magnetic unit cell of FeGaGe is six times larger than the nuclear unit cell. The antiferromagnetic structure has no net magntic moment and is noncollinear. Its main feature is that the spins along the quasi-1D Fe chains have periodic modulation along the chain-direction, forming a circular oblique cycloid. For the other two magnetic models with similar refinement R-factors, Fig. S1 and S2 show that their magnetic structures are slightly different in the circular plane or canting angle, but both retain the circular spin cycloid feature along the quasi-1D Fe chains. More details can also be found in the `.mcif` files in the supplemental material. It should be noted that due to the resolution limit, the difference in the diffraction data between 3.5 K and 100 K cannot be resolved. Finally, it also should be noted that the current powder neutron data cannot provide an unambiguous determination of the magnetic structure, for instance, whether k-vector is commensurate or not. Single crystal neutron diffraction is necessary for further clarification.

C. Discussion

The above results have shown several intriguing features in the structure and physical properties of FeGaGe. Firstly, the quasi-1D Fe chains are interlaced with an intersection angle of 60 degrees between layers along the c axis. This makes FeGaGe a intriguing example among all well-known quasi-1D spin-chain systems. Secondly, although our neutron diffraction data failed to resolve any differences below and above T^*, the electrical transport data indeed exhibit non-negligible features across T^*, which makes another important point that may attract further investigations. Finally, based on a detailed analysis of the neutron diffraction data, our results provide evidence for a possible circular spiral magnetic

order in FeGaGe. In quasi-1D materials, spiral or helical magnetic modulations typically arise from specific structural architectures and exchange constraints. For instance, helical orders observed in cluster-type chains like $RbMn_6Bi_5$[47], or driven by interchain geometric frustration in structures with interchain triangular motifs, such as $MnBi_2Se_4$[48]. Alternatively, in classical quantum spin chains like $LiCuVO_4$ and $PbCuSO_4(OH)_2$, helical and elliptical modulations are fundamentally governed by the strong competition between intrachain nearest-neighbor ferromagnetic and next-nearest-neighbor antiferromagnetic interactions[49, 50]. For FeGaGe possesses single-atom and nearly linear Fe chains, the realization of a circular spiral within such an architecture is unusual. Furthermore, the remarkably high magnetic ordering temperature ($T_N \sim 130$ K) firmly underscores the presence of substantial interchain magnetic coupling. Therefore, the spiral ground state in FeGaGe is unlikely to originate solely from isolated intrachain frustration; rather, it points to a possible delicate competition between intrachain and interchain magnetic interactions. On the other hand, the Ga/Ge site-mixing in FeGaGe could possibly break its spatial inversion symmetry and give rise to Dzyaloshinskii-Moriya interaction, then serve as another possible mechanism for the non-collinear magnetic structure. In any case, the periodic modulation of spins along these linear quasi-1D Fe chains indicates an exotic magnetic ground state, establishing FeGaGe as a compelling platform for further exploring itinerant magnetic frustration and novel quantum magnetic phenomena.

IV. CONCLUSIONS

In summary, based on the successful growth of both polycrystalline samples and single crystals of FeGaGe, its structural and physical properties were investigated. FeGaGe features quasi-1D interlaced Fe chains. Besides the previously known antiferromagnetic transition at $T_N \sim 130$ K, additional susceptibility anomaly and magnetotransport feature at $T^* \sim 60$ K are identified. Neutron diffraction study on FeGaGe reveals a possible circular spiral magnetic structure with the circular spin cycloid feature along the quasi-1D Fe chains. Our findings make FeGaGe an important material platform for further exploring exotic quantum magnetic states.

ACKNOWLEDGEMENT

This work was supported by the National Natural Science Foundation of China (No. 12474148 and No. 12074426)

[1] Broholm C, Cava R J, Kivelson S A, Nocera D G, Norman M R and Senthil T 2020 *Science* **367** eaay0668

[2] Li Y, Chen G, Tong W, Pi L, Liu J, Yang Z, Wang X and Zhang Q 2015 *Phys. Rev. Lett.* **115** 167203

[3] Shen Y, Li Y D, Wo H, Li Y, Shen S, Pan B, Wang Q, Walker H C, Steffens P, Boehm M, Hao Y, Quintero-Castro D L, Harriger L W, Frontzek M D, Hao L, Meng S, Zhang Q, Chen G and Zhao J 2016 *Nature* **540** 559–562

[4] Zeng Z, Zhou C, Zhou H, Han L, Chi R, Li K, Kofu M, Nakajima K, Wei Y, Zhang W, Mazzone D G, Meng Z Y and Li S 2024 *Nat. Phys.* **20** 1097–1102

[5] Lin G and Ma J 2023 *The Innovation* **4** 100484

[6] Sheng J, Wang L, Candini A, Jiang W, Huang L, Xi B, Zhao J, Ge H, Zhao N, Fu Y, Ren J, Yang J, Miao P, Tong X, Yu D, Wang S, Liu Q, Kofu M, Mole R, Biasiol G, Yu D, Zaliznyak I A, Mei J W and Wu L 2022 *Proc. Natl. Acad. Sci. U.S.A.* **119** e2211193119

[7] Xiang J, Zhang C, Gao Y, Schmidt W, Schmalzl K, Wang C W, Li B, Xi N, Liu X Y, Jin H, Li G, Shen J, Chen Z, Qi Y, Wan Y, Jin W, Li W, Sun P and Su G 2024 *Nature* **625** 270–275

[8] Shu M, Xu X, Xi N, He M, Xiang J, Qu G, Khalyavin D, Manuel P, Nakamura J G, Jiao J, Liu Y, Wu G, Guo K, Zhao H, Xu W, Duan Q, Zhong R, Wang X, Han Y, Ling L, Sun X, Song D, Gao Y, Wang Z, Chen X, Qian

T, Jia S, Du H, Su G, Li W, Ma J and Qu Z 2026 *Nature* **651** 61–67

[9] Kamiya Y, Ge L, Hong T, Qiu Y, Quintero-Castro D L, Lu Z, Cao H B, Matsuda M, Choi E S, Batista C D, Mourigal M, Zhou H D and Ma J 2018 *Nat. Commun.* **9** 2666

[10] Ran K, Wang J, Wang W, Dong Z Y, Ren X, Bao S, Li S, Ma Z, Gan Y, Zhang Y, Park J T, Deng G, Danilkin S, Yu S L, Li J X and Wen J 2017 *Phys. Rev. Lett.* **118** 107203

[11] Yu Y J, Xu Y, Ran K J, Ni J M, Huang Y Y, Wang J H, Wen J S and Li S Y 2018 *Phys. Rev. Lett.* **120** 067202

[12] Zheng J, Ran K, Li T, Wang J, Wang P, Liu B, Liu Z X, Normand B, Wen J and Yu W 2017 *Phys. Rev. Lett.* **119** 227208

[13] Lin G, Jeong J, Kim C, Wang Y, Huang Q, Masuda T, Asai S, Itoh S, Günther G, Russina M, Lu Z, Sheng J, Wang L, Wang J, Wang G, Ren Q, Xi C, Tong W, Ling L, Liu Z, Wu L, Mei J, Qu Z, Zhou H, Wang X, Park J G, Wan Y and Ma J 2021 *Nat. Commun.* **12** 5559

[14] Yao W, Iida K, Kamazawa K and Li Y 2022 *Phys. Rev. Lett.* **129** 147202

[15] Jin X, Geng M, Orlandi F, Khalyavin D, Manuel P, Liu Y and Li Y 2025 *Phys. Rev. Lett.* **135** 136701

[16] Xu H H, Liu Q Y, Xin C, Shen Q X, Luo J, Zhou R, Cheng J G, Liu J, Tao L L, Liu Z G, Huo M X, Wang X J and Sui Y 2024 *Chinese Physics B* **33** 037505

[17] Jiang L, Jiang C Y, Tian Y C, Zhao H, Zhang J, Y T Z, Fu S H, Liang E J, Wang X C, Jin C and Zhao J 2024 *Chinese Physics Letters* **41** 047802

[18] He Z, Taniyama T, Kyômen T and Itoh M 2005 *Phys. Rev. B* **72** 172403

[19] Zou H, Cui Y, Wang X, Zhang Z, Yang J, Xu G, Okutani A, Hagiwara M, Matsuda M, Wang G, Mussardo G, Hódsági K, Kormos M, He Z, Kimura S, Yu R, Yu W, Ma J and Wu J 2021 *Phys. Rev. Lett.* **127** 077201

[20] Wu L S, Gannon W J, Zaliznyak I A, Tsvelik A M, Brockmann M, Caux J S, Kim M S, Qiu Y, Copley J R D, Ehlers G, Podlesnyak A and Aronson M C 2016 *Science* **352** 1206–1210

[21] Zhang S S, Wang Z A, Li B, Jiang Y Y, Zhang S H, Xiao R C, Liu L X, Luo X, Lu W J, Tian M, Sun Y P, Tsymbal E Y, Du H and Shao D F 2025 *Newton* 100068

[22] Radzihovsky L and Pellett E 2025 *Phys. Rev. Lett.* **135** 016001

[23] Yin J X, Lian B and Hasan M Z 2022 *Nature* **612** 647–657

[24] Neupert T, Denner M M, Yin J X, Thomale R and Hasan M Z 2022 *Nat. Phys.* **18** 137–143

[25] Fu L, Cheng W, Shi L, Min B, Peng Y, Zhang J, Song J, Deng Z, Zhao J, Liu Y, Zhu J, Zhang J, Wang X and Jin C 2026 *Chinese Physics Letters* **43** 010705

[26] Pandey A, Miao P, Klemm M, He H, Wang H, Qian X, Lynn J W and Aronson M C 2020 *Phys. Rev. B* **102** 014406

[27] Li X Y, Nocera A, Foyevtsova K, Sawatzky G A, Oudah M, Murai N, Kofu M, Matsuura M, Tamatsukuri H and Aronson M C 2025 *Nat. Mater.* **24** 716–721

[28] Malaman B, Le Caër G, Philippe M and Roques B 1976 *Mater. Res. Bull.* **11** 787–792

[29] Cheng P, Zhang H, Bao W, Schneidewind A, Link P, Grünwald A, Georgii R, Hao L and Liu Y 2016 *Nucl. Instrum. Methods Phys. Res. Sect. A* **821** 17–22

[30] Sun S, Xu D, Shang C, Shi B, Huang J, Gui X, Sun Z, Liu J, Wang J, Zhang H and Cheng P 2025 *J. Alloys Compd.* **1036** 181507

[31] Shi B, Geng Y, Wang H, Yang J, Shang C, Wang M, Mi S, Huang J, Pan F, Gui X, Wang J, Liu J, Xu D, Zhang H, Qin J, Wang H, Hao L, Tian M, Cheng Z, Zheng G and Cheng P 2024 *J. Am. Chem. Soc.* **146** 21546–21554

[32] Teng X, Chen L, Ye F, Rosenberg E, Liu Z, Yin J X, Jiang Y X, Oh J S, Hasan M Z, Neubauer K J, Gao B, Xie Y, Hashimoto M, Lu D, Jozwiak C, Bostwick A, Rotenberg E, Birgeneau R J, Chu J H, Yi M and Dai P 2022 *Nature* **609** 490–495

[33] Wen X, Zhang Y, Li C, Gui Z, Li Y, Li Y, Wu X, Wang A, Yang P, Wang B, Cheng J, Wang Y, Ying J and Chen X 2024 *Physical Review Research* **6** 033222

[34] Lin X, Bondarenko V, Cao G and Brill J 2004 *Solid State Communications* **130** 151–154

[35] Khalaniya R A, Verchenko V Y, Mironov A V, Samarin A N, Bogach A V, Kulchu A N, Polevik A O, Wei Z, Dikarev E V, Stern R and Shevelkov A V 2025 *Dalton Transactions* **54** 8317–8330

[36] Shang C, Xu D, Shi B, Gui X, Sun Z, Liu J, Wang J, Zhang H, Wang H, Hao L and Cheng P 2026-05-07 *Phys. Rev. B* **113** 184430

[37] Aroyo M I, Perez-Mato J M, Capillas C, Kroumova E, Ivantchev S, Madariaga G, Kirov A and Wondratschek H 2006 *Z. Kristallogr. Cryst. Mater.* **221** 15–27

[38] H T Stokes D M H and Campbell B J *iso.byu.edu*

[39] Campbell B J, Stokes H T, Tanner D E and Hatch D M 2006 *J. Appl. Crystallogr.* **39** 607–614

[40] Petříček V, Palatinus L, Plášil J and Dušek M 2023 *Z. Kristallogr. Cryst. Mater.* **238** 271–282

[41] Perez-Mato J, Gallego S, Tasci E, Elcoro L, De La Flor G and Aroyo M 2015 *Annu. Rev. Mater. Res.* **45** 217–248

[42] Pan F, Hu X, Huang J, Shi B, Wang J, Liu J, Zhang H, Xu D, Qin J, Wang H, Hao L, Cao K, Cheng P and Yao D X 2023 *Phys. Rev. B* **107** 224423

[43] Huang J, Shang C, Qin J, Pan F, Shi B, Wang J, Liu J, Xu D, Zhang H, Wang H, Hao L, Bao W and Cheng P 2023 *Phys. Rev. B* **108** 184431

[44] Tian C K, Wang C, Ji W, Wang J C, Xia T L, Wang L, Liu J J, Zhang H X and Cheng P 2019 *Phys. Rev. B* **99** 184428

[45] Tian C, Pan F, Xu S, Ai K, Xia T and Cheng P 2020 *Appl. Phys. Lett.* **116** 202402

[46] Sheng J, Li X, Tian C, Song J, Li X, Sun G, Xia T, Wang J, Liu J, Xu D, Zhang H, Tong X, Luo W, Wu L, Bao W and Cheng P 2020 *Phys. Rev. B* **101** 174516

[47] Chen L, Zhao L, Qiu X, Zhang Q, Liu K, Lin Q and Wang G 2021 *Inorg. Chem.* **60** 12941–12949

[48] Clark J, Pak C, Cao H and Shatruk M 2021 *Crystals* **11** 242

[49] Enderle M, Mukherjee C, Fåk B, Kremer R K, Broto J M, Rosner H, Drechsler S L, Richter J, Malek J, Prokofiev A, Assmus W, Pujol S, Raggazzoni J L, Rakoto H, Rheinstädter M and Rønnow H M 2005 *Europhys. Lett.* **70** 237–243

[50] Willenberg B, Schäpers M, Rule K C, Süllow S, Reehuis M, Ryll H, Klemke B, Kiefer K, Schottenhamel W, Büchner B, Ouladdiaf B, Uhlarz M, Beyer R, Wosnitza J and Wolter A U B 2012 *Phys. Rev. Lett.* **108** 117202